JTTEE5 23:676–683
DOI: 10.1007/s11666-014-0056-7
1059-9630/$19.00 © ASM International

Al/Al_2O_3 Composite Coating Deposited by Flame Spraying for Marine Applications: Alumina Skeleton Enhances Anti-Corrosion and Wear Performances

Jing Huang, Yi Liu, Jianhui Yuan, and Hua Li

(Submitted September 5, 2013; in revised form December 1, 2013)

Here we report aluminum-alumina composite coatings fabricated by flame spraying for potential marine applications against both corrosion and wear. Microstructure examination suggested dense coating structures and the evenly distributed alumina splats formed hard skeleton connecting individual Al splats. The anti-corrosion and wear performance of the coatings were enhanced significantly by the addition of alumina. Failure analyses of the coatings after accelerated corrosion testing disclosed the intact alumina skeleton, which prevented further advancement of the corrosion. The results suggest that there is great potential for the cost-effective Al-Al_2O_3 coatings with tailorable alumina contents for application in the marine environment.

Keywords aluminum, alumina, composite coating, corrosion, flame spraying

1. Introduction

The booming ocean economy in recent decades crucially demands advanced anti-corrosion technologies for marine infrastructures (Ref 1, 2). Cost-effective metals such as carbon and HSLA steels have been widely used for constructing marine structures (Ref 3). Steel constructions, such as drilling platforms and sea bridges, encounter severe corrosion damage in the marine environment (Ref 4), among which the splash zone is generally considered to be the most corrosive environment (Ref 5, 6). Nowadays, the most effective strategy for mitigating corrosion is coating technique, since coatings on marine structures are capable of accomplishing sacrificial corrosion protection, physical isolation protection, etc (Ref 2, 7, 8). Numerous methods have been developed for fabricating the protective coatings, and the most extensively used protecting technique against marine corrosion is the use of organic coatings (Ref 9, 10). However, corrosion progression in the defects inherent in organic coatings affects their functional service life (Ref 2, 9). Thermal spraying offers the advantages of cost efficiency, wide selection of coating materials, easy on-site operation, etc., making it one of the most promising methods in surface engineering. Extensive studies have shown competitive capabilities of thermal sprayed coatings in protecting ocean structures from corrosion in a long term (Ref 11). Multiple thermal spray methods were successfully employed for making the coatings, such as arc spray (Ref 2), high velocity oxy-fuel (HVOF) spray (Ref 12–15), or flame spray (Ref 16). Among the thermal sprayed coatings, aluminum coatings proved to be the most economical corrosion protection system for the marine environment (Ref 17). However, use of aluminum coatings is limited, since in most cases marine corrosion always accompanies wear (Ref 18). On-site exposure testing has already clearly shown that the well-performed coatings in less-wear environment did not meet the demands for protection in the splash zone (Ref 19), which involves more wear-associated erosion. Carbide coatings have, therefore, been developed to combat both the corrosion and wear in marine engineering (Ref 20). The coatings, however, raise cost issues, since they are usually deposited by expensive HVOF process (Ref 12–15). Alternative wire arc spray or flame spray technique is much cheaper, but the coatings are poor in wear resistance. Novel coatings deposited by efficient approaches for combined super corrosion/wear resistance are needed.

Understanding the failure mechanism is essential for selecting appropriate coating materials and designing the coating structure to resist damage in the marine environment. As one of the key reasons accounting for the failure of steel structures in the marine environment, corrosion is usually categorized into two basic types, namely galvanic corrosion and stray current corrosion, both of which are related to electrochemical corrosion (Ref 2, 21, 24). Despite the electrochemical reaction-induced corrosion, due to its higher corrosion potential than iron, aluminum

Jing Huang, Yi Liu, Jianhui Yuan, and **Hua Li**, Key Laboratory of Marine Materials and Related Technologies, Zhejiang Key Laboratory of Marine Materials and Protective Technologies, Ningbo Institute of Materials Technology and Engineering, Chinese Academy of Sciences, Ningbo 315201, China. Contact e-mail: lihua@nimte.ac.cn.

coating performed well as the barrier and in turn achieved sacrificial protection (Ref 7, 8). However, the erosion caused by hard particles for instance sand in flowing seawater is usually very serious, leading to accelerated corrosion and consequent damage of the coatings. Corrosion-erosion processes are vastly investigated due to the devastating effects that are observed in materials. For metals, corrosion-erosion processes affect engineered structures such as pipes, diaphragms, offshore to energy conversion, and many others for marine applications (Ref 22, 23). When corrosion and erosion play together, the damage of the materials is further deteriorated and the degradation mechanisms are complex (Ref 24). When metal is subjected to hard particle impact, erosion causes rupture or removal of the protective film from the metal surface, leaving the metallic substrate exposed to erosive solution (Ref 25). Protective coatings with excellent anti-corrosion and pronounced anti-wear performances are, therefore, required. Alumina (Al_2O_3), a typical hard ceramic with outstanding properties like low density, high strength, high wear resistance, and excellent chemical stability, is of tremendous potential in the field of anti-friction/wear applications (Ref 26, 27). In this paper we proposed a flame sprayed composite coating with enhanced corrosion and wear resistance for potential marine applications. The composite coatings were deposited by flame spraying pre-mixed Al-Al_2O_3 feedstock powder. Microstructural characterization of the coatings suggested even distribution of Al_2O_3 splats in the coatings and the splats formed a hard skeleton, preventing effectively further progress of corrosion. In addition, the existence of Al_2O_3 at the coating surfaces significantly reinforced wear resistance. The strengthening mechanism in both the corrosion and wear resistance was elucidated.

2. Materials and Methods

2.1 Deposition of the Coatings

Commercially available powder of aluminum (Al, Beijing General Research Institute of Mining and Metallurgy, China) and alumina (Beijing Sangyao Technology Co., China) with the size range of +50-100 and +15-45 μm, respectively, were used in this study. Previous preliminary study on Al-Al_2O_3 coatings (10 wt.%Al_2O_3, 20 wt.% Al_2O_3, 30 wt.%Al_2O_3, 40 wt.%Al_2O_3, 60 wt.%Al_2O_3, 80 wt.%Al_2O_3) showed that 20 wt.% of Al_2O_3 was the best percentage for anti-corrosion/wear performances of the flame sprayed Al-based coatings. For deposition of the Al-Al_2O_3 coating, the Al (80 wt.%) and Al_2O_3 (20 wt.%) powder were pre-mixed and mechanically blended. To avoid uneven distribution of the components in the as-sprayed coatings, the mixed powder was stirred using compressed air during powder feeding. Mild steel plates with the dimension of 50 × 30 × 4 mm^3 were used as the substrates for the coating deposition. Prior to the spraying, the substrates were surface grit blasted using 60 mesh black fused alumina sand and subsequently degreased by sonication cleaning in acetone. For comparison purpose, the Al-Al_2O_3 coatings were deposited by flame spray process (FS-4 system, Wuhan Research Institute of Materials Protection, China) and the pure Al coatings were deposited by both flame spray and high velocity arc spray (AS, TLAS-500C, China). The flame spray system was specially designed for making coatings of metal alloys and ceramics. For the flame spraying, acetylene was used as the fuel gas with the flow rate of 1.5 Nm^3/h and working pressure of 0.1 MPa. Pressure and flow rate of oxygen were 0.5 MPa and 2.5 Nm^3/h, respectively. The powder feed rate was 30 g/min and spray distance was 20 cm. For the arc spraying, the current and voltage of the arc were set at 80-100 A and 25 V, respectively, and the spray distance was 15 cm. The compressed air with the pressure of 0.5 MPa was used for the arc spraying.

2.2 Testing Methods

Phases in the powder and the coatings were detected by x-ray diffraction (XRD, PANalytical X'pert Pro MPD diffractometer, The Netherlands) at a scan rate of 0.02°/s over a 2θ range of 20°-80° using Cu Kα radiation operated at 35 mA and 40 kV. Topographical and cross-sectional morphology of the coatings was examined by field emission scanning electron microscope (FESEM, Hitachi S-550N, Japan). Element analyses were carried out by using energy dispersive x-ray spectra (EDX) equipped with the FESEM. The porosity of the coatings was measured using the Brunauer, Emmett and Teller (BET) method by adsorption of nitrogen gas on ASAP 2020 M apparatus at 77.3 K, and the BET surface area was calculated over the relative pressure range of 0.05-0.20 MPa. For assessing the corrosion resistance of the coatings, the neutral salt spray (NSS) testing was conducted according to the ASTM B117/90 standard (Ref 28). The assessments were performed using standardized 5% NaCl solution with the pH value of 6.7-7.2 at room temperature. For polarization test, the coating samples with the surface area of 15 × 10 mm^2 were exposed to 3 wt.% NaCl solution (Ref 21). The polarization curves acquired by scanning the potential at a rate of 0.01 V/s from −1.5 to 0.5 V were recorded on an electrochemical workstation (M273A, PARC, USA). A similar copper accelerated acetic acid salt spray testing was also conducted to disclose the corrosion failure mechanisms of the coatings. For the solution preparation, one gram of copper chloride dehydrate was added to 3.8 l of 5% NaCl solution and the pH value of the work solution was 3.0 as being adjusted through adding acetic acid. All the coating samples polished using 1200 mesh sand paper were immersed in the 40 °C copper accelerated acetic acid salt solution for several days.

Tribological properties of the coatings were evaluated using a reciprocating-type ball-on-disk tribometer (JLTB-02, J&L Tech Co. Ltd, Korea), which was equipped with an environmental chamber where the relative humidity and gaseous environment can be controlled (Ref 29). The tests were performed at room temperature with the relative humidity of 70% under a load of 5 N and an average sliding speed of 120 mm/s for 420 s. 304 stainless steel balls with the diameter of 3.5 mm were used as the

counterparts. The coatings and 304 balls were ultrasonically cleaned in acetone prior to the testing and a new ball or a new position of the ball was used for each friction test. The friction coefficients and sliding time were automatically recorded during the tests. The test for each sample was repeated three times at least. After the tests, wear volume was measured using a profile tester (Alpha-Step IQ, USA) and wear rate was calculated from the following relationships (Ref 29):

$$k = \frac{V}{L \times D} \quad \text{(Eq 1)}$$

$$V = S \times H \quad \text{(Eq 2)}$$

where K is wear rate, V is wear volume, L is applied normal load, D is sliding distance, S is cross-sectional area of wear zone, and H is wear distance.

3. Results and Discussion

3.1 Microstructure of the Coatings

Dense structure was achieved for the coatings deposited by both the flame spraying (FS) and AS (Fig. 1). Dense structure is suggested from their cross-sectional views. Further, porosity measurement by BET approach showed the average porosity of 1.53, 8.29, and 2.61% for the AS Al coating, the FS Al coating, and the FS Al-Al_2O_3 coating, respectively. Compared with the FS Al coating, the composite coating is much denser. For the Al-Al_2O_3 composite coatings, it is clear that alumina splats are evenly distributed in the coating (Fig. 1c), showing undetectable flaws at Al/Al_2O_3 interfaces. XRD detection suggests negligible oxidation of Al during the AS deposition (Fig. 2). However, the FS Al coating exhibits weak peaks for Al_2O_3, indicating oxidation of certain amount of Al during the spraying, which is likely attributed to the longer dwelling time of Al droplets before flattening/solidification upon impingement on pre-coating/substrate. Due to the inert nature of alumina, its uniform presence in the FS Al coating could enhance the anti-corrosion properties. Compared to the starting Al-Al_2O_3 powder, the FS Al-Al_2O_3 coating shows the major structure changes of Al_2O_3 from α-Al_2O_3 in the starting powder to γ-$A1_2O_3$ in the coating. The appearance of γ-$A1_2O_3$ in the coating reflects the molten state of the powder during the spraying (Ref 30, 31). The partially melted $A1_2O_3$ particles may enhance the interfaces between Al and $A1_2O_3$, giving rise to improved coating performances.

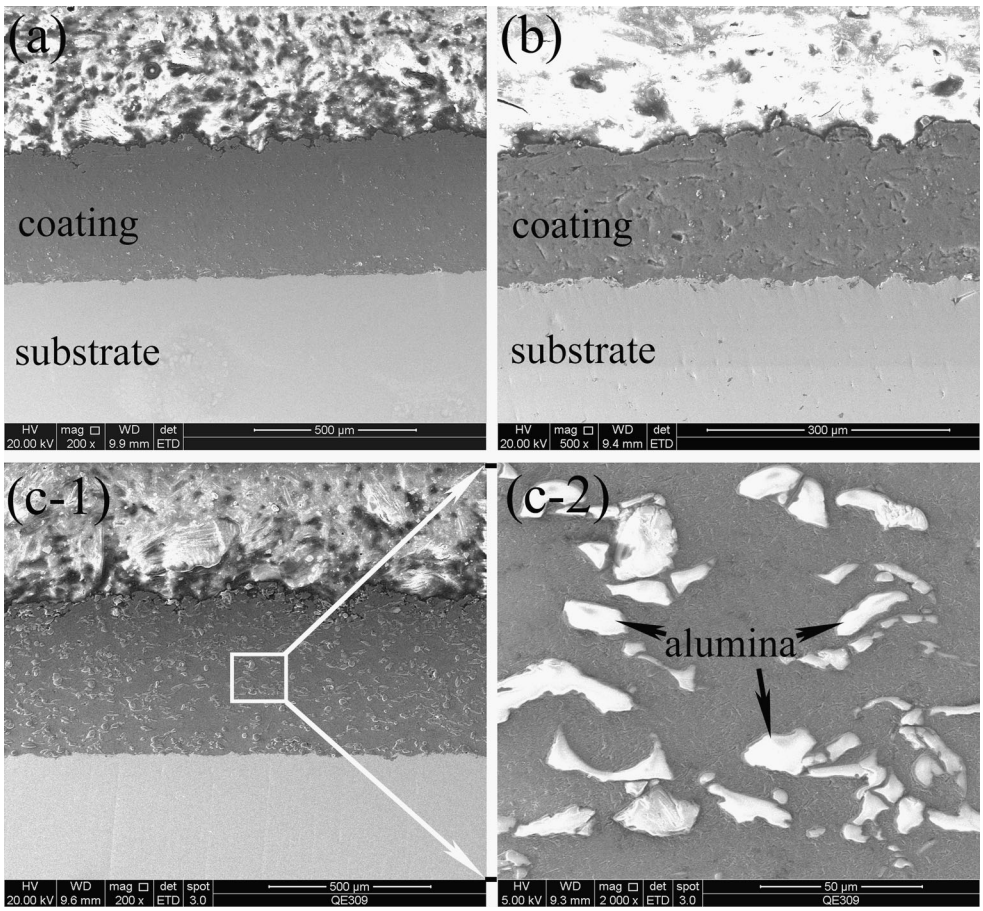

Fig. 1 Cross-sectional FESEM views of the Al and Al-Al_2O_3 coatings deposited by FS and AS, (a) the AS Al coating, (b) the FS Al coating, and (c) the FS Al-Al_2O_3 coating

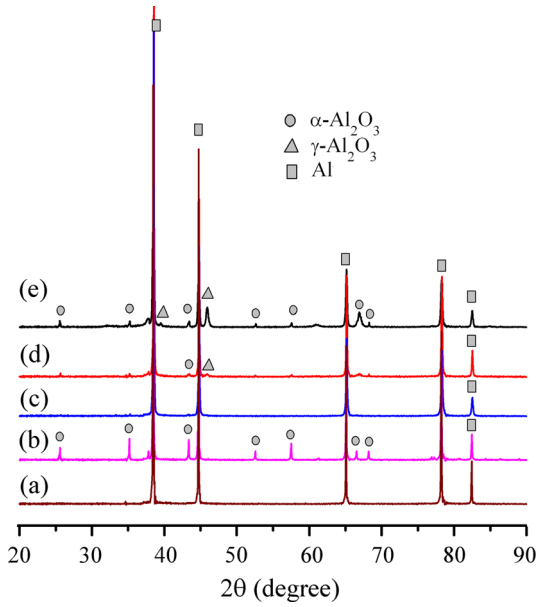

Fig. 2 XRD patterns of (a) the starting Al powder, (b) the Al-20 wt.%Al_2O_3 powder, (c) the AS Al coating, (d) the FS Al coating, and (e) the FS Al-Al_2O_3 coating

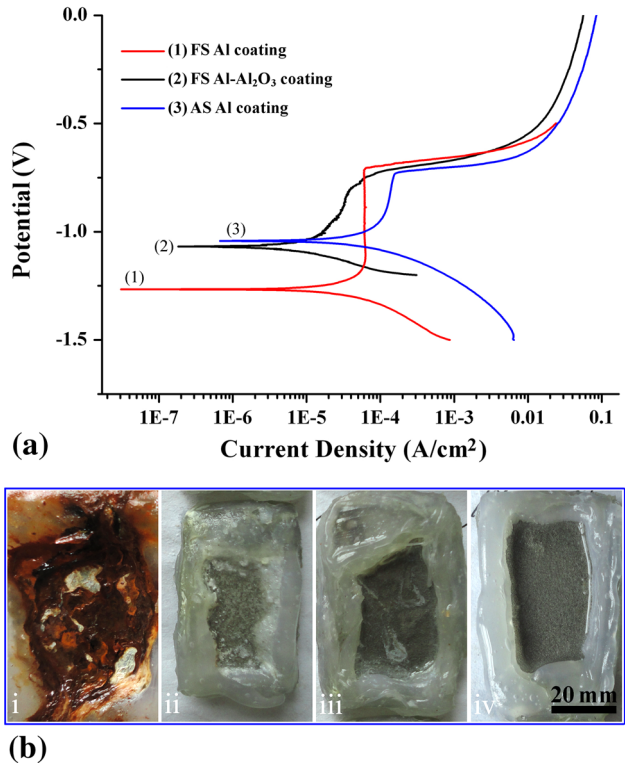

Fig. 3 Anti-corrosion testing results of the coatings, (a) potentiodynamic polarization curves for the pure Al coatings and the Al-Al_2O_3 coating measured in 3% NaCl solution, and (b) the digital photos of the coatings after 1155 h of neutral salt spray test (NSS test) showing effective protection of the coatings against corrosion (i: mild steel plate without coating, ii: the AS Al coating, iii: the FS Al coating, and iv: the FS Al-Al_2O_3 coating)

3.2 Corrosion Resistance of the Coatings

It was well established that corrosion resistance of materials is closely related to their corrosion potential and corrosion current density (Ref 32). The potentiodynamic polarization curves of the coating samples acquired in 3% NaCl solution show that the FS Al coating has a fairly negative corrosion potential at −1.263 V (Fig. 3a), which is comparable to the values reported by Rodriguez et al. (Ref 32). The corrosion potentials of the FS Al-Al_2O_3 coating and the AS Al coating show increased values, −1.068 and −1.036 V, respectively. Surprisingly, the corrosion current density of the FS Al-Al_2O_3 composite coating, 2.727×10^{-6} A/cm^2, is significantly lower than that of FS Al coating, 7.079×10^{-6} A/cm^2, or AS Al coating, 1.026×10^{-5} A/cm^2. This implies that addition of Al_2O_3 has already enhanced markedly the corrosion resistance of the Al-based coatings. To further investigate the anti-corrosion performances of the coatings, they were subjected to the NSS test. After 1155 h testing, the mild steel plate without coating on it exhibits a lot of rusty corrosion products, indicating severe corrosion (Fig. 3b). The Al-Al_2O_3 composite coating shows the best performance among the coatings that there are no white corrosion products visible, while the corrosion products in flocculent form are clearly seen on the pure Al coatings.

Progress has been made in understanding the failure mechanisms of thermal sprayed coatings in corrosive environment. In this study, corrosion regimes of the aluminum and aluminum-alumina coatings were investigated by the accelerated corrosion testing. The typical surface morphologies of the coatings before and after the immersion are shown in Fig. 4. Numerous holes induced by corrosion are clearly seen on the surfaces of the coatings. After 144 h corrosion testing, severe pitting corrosion is suggested for the pure Al coatings (Fig. 4a-2, b-2). Surprisingly, even after 408 h immersion, the Al-Al_2O_3 coating exhibits intact alumina splats on its surface (Fig. 4c-2). Most of the aluminum splats have already been corroded away (as indicated by the holes shown in Fig. 4c-2 vs. c-1), leaving well-retained alumina splats.

Further morphological examination from the cross-sections of the coatings after the accelerated corrosion evidences progressing path of the corrosion along the through-thickness direction from their surfaces all the way down to the substrate (Fig. 5a). Strikingly, apart from their isolated presence alone, the alumina splats connect with each other, forming a skeleton-like structure (Fig. 5a). Major part of the aluminum splats located in between alumina splats were corroded away, but those closely contacting with alumina splats are still there. It, therefore, suggests that the corrosion, in particular pitting corrosion, is initiated predominately from the areas of aluminum splats without contact with alumina splats. Compared to those areas, the Al/Al_2O_3 interfaces are strong in resisting the corrosion. The materials most susceptible to pitting corrosion are usually the ones where

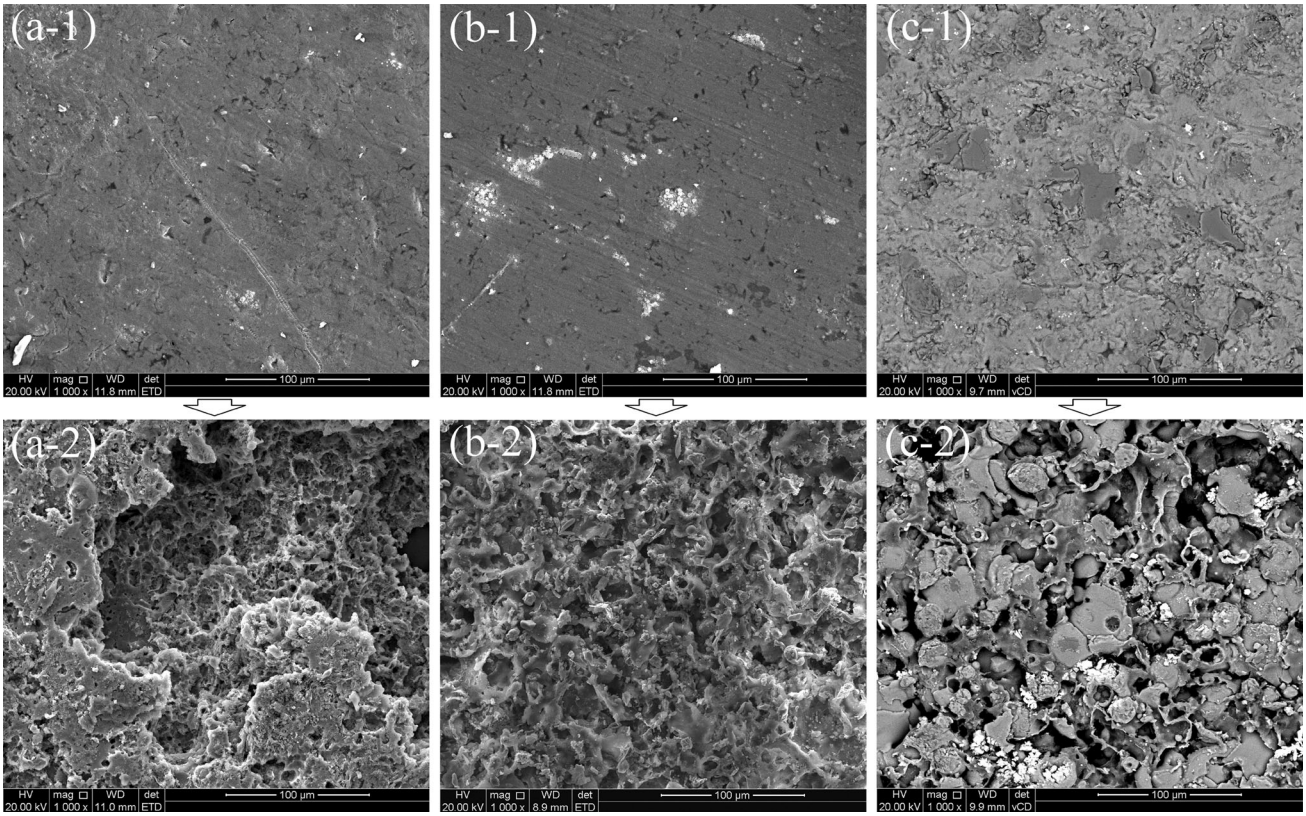

Fig. 4 Typical surface morphologies of the coatings before (−1) and after (−2) the immersion in the copper accelerated acetic acid salt solution showing the preferred corrosion of Al and intact Al_2O_3 splats after the testing, (a-1, a-2) the AS Al coating, (b-1, b-2) the FS Al coating, and (c-1, c-2) the FS Al-Al_2O_3 coating. The pure Al coatings (a, b) were immersed in the testing solution for 144 h, while the FS Al-Al_2O_3 coating (c) was immersed for 408 h

corrosion resistance is caused by a passivation layer (Ref 33). Aluminum is basically active metal, a thin surface passivation layer of aluminum oxide has been revealed in the coatings by the XRD detection (Fig. 2). The oxide should be located at periphery of aluminum splat, most likely accounting for the observed phenomena that the Al/Al_2O_3 interfaces are more anti-corrosive. It was claimed that in Ni-Al_2O_3 composite coating, passivation is facilitated by nonconducting alumina particles co-deposited with nickel, which contributes to formation of active centers with increased oxygen adsorption (Ref 34), in turn resulting in increase in anti-corrosion performances. The current results agree well with those reported findings. Based on the microstructural features and elucidation, a schematic model illustrating the corrosion of the Al/Al_2O_3 coating is proposed (Fig. 5b). The unique distribution of alumina splats in the coating (left half of Fig. 5b) gives rise to the formation of alumina skeleton that remains almost intact after the corrosion test (right half of Fig. 5b). As disclosed by the SEM characterization, the extent of the corrosion at top surfaces of the coatings is most remarkable. Cl^- ions in the solution are the main factor causing corrosion (Ref 35, 36). The ions hinder possible formation of a film of oxides on the surface of aluminum and in turn destroy the already formed passive layers (Ref 36), resulting in local corrosion, i.e., pitting corrosion in this case. When the pits are generated, the Cl^- ions become concentrated in the pits for charge neutrality and encourage the reaction of positive Al^{3+} with water to form a hydroxide corrosion product and H^+ ions (Ref 37). For the current Al/Al_2O_3 composite coating, the alumina skeleton structure cuts off the penetration path of Cl^- ions into the inside of the coating, in turn slowing down the advancement of the corrosion.

3.3 Anti-Wear Performances of the Coatings

The friction coefficient of the pure Al coatings at stable wear state (either the FS Al coating or the AS Al coating) is ~0.50, while the composite coating shows a value of ~0.52 (Fig. 6a). The increase in friction coefficient values is normal for the composites consisting of hard particles (Ref 38–40). Significantly reduced wear rate was realized for the alumina-containing coating (Fig. 6b). The wear rate of the Al-Al_2O_3 coating, 8.93×10^{-4} $mm^3/N/m$, is about one fifth of those of the pure aluminum coatings.

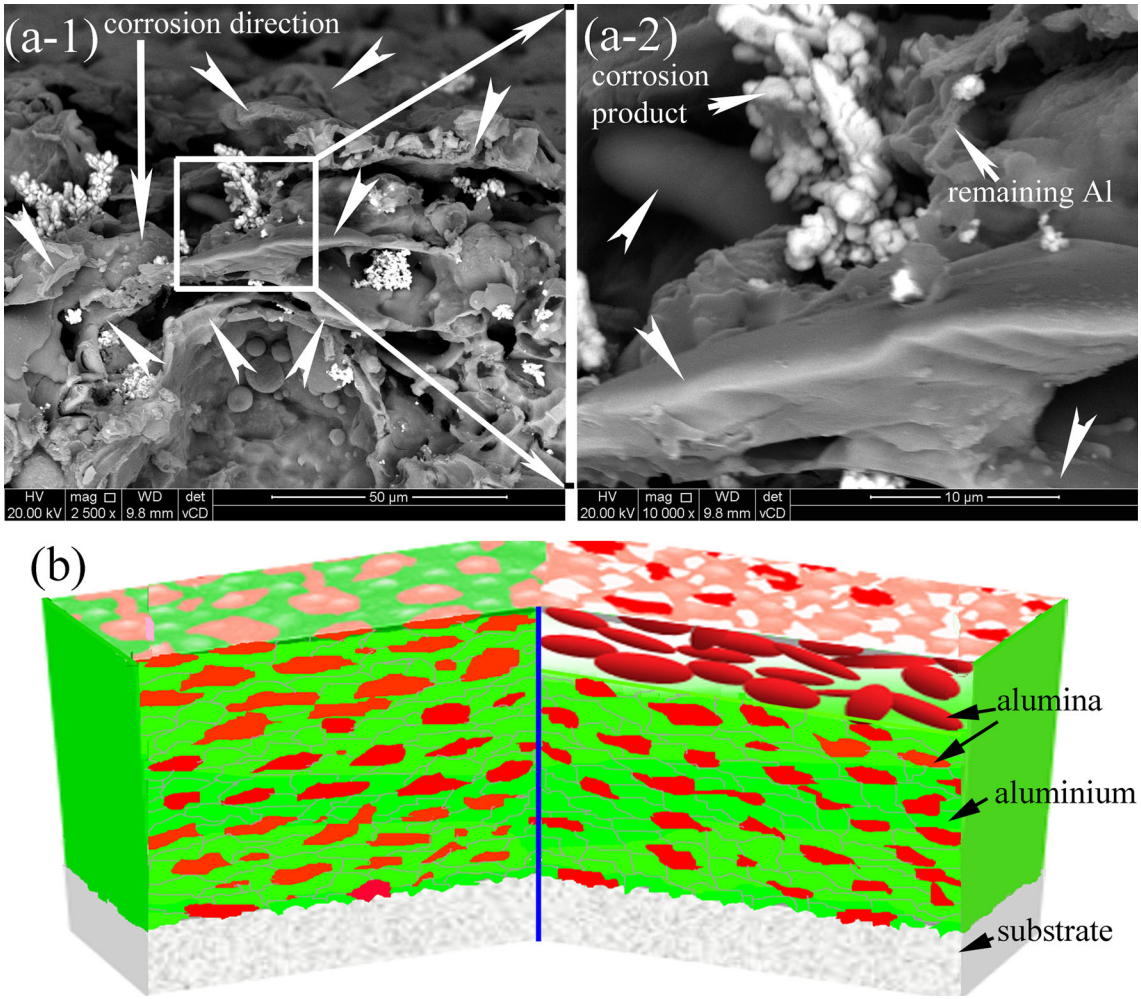

Fig. 5 Cross-sectional morphology of the Al-Al_2O_3 coating after the accelerated corrosion testing showing an inert skeleton structure constructed by alumina splats (a, a-2 is the magnified view of selected area in a-1), the skeleton resists effectively further progression of the corrosion (the substance in white color is the corrosion product), and (b) schematic depiction showing the mechanism as to how the Al_2O_3 skeleton in the coating resists advancement of corrosion

There is no significant difference in the wear rate and friction coefficient between the FS Al coating and the AS Al coating. It is noted that the wear morphology of the Al-Al_2O_3 coating differs from that of the pure Al coatings (Fig. 6c). Microcracks and deep plowing grooves are observed on the wear tracks of the Al coatings. More plowed marks were observed on the wear track of the materials having relatively higher values of wear rate and lower hardness values (Ref 41). In fact, the deep plowing grooves, ridges, and chips observed on the wear tracks of the Al coatings are the features of adhesive wear-dominated regimes (Ref 41, 42). While the composite coating shows the wear tracks with relatively narrow width and shallow plowing grooves. Further close microstructural examination evidenced the predominating fretting wear, apart from secondary adhesive wear, for the alumina-containing coating. The worn morphologies are consistent with the wear rates of the coatings. Addition of more alumina into the Al-based coating, for example, 50 wt.% alumina, not only resulted in further enhanced wear resistance, but also introduced the issues of high brittleness and poor cohesion of the coatings (data not shown). Balance among anti-corrosion, anti-wear, and other mechanical properties are one of the primary concerns for design and fabrication of the Al-Al_2O_3 coating for marine applications. The current cost-effective flame spraying has limitations in spraying ceramic materials, mainly due to the relatively low flame temperature, ~2000-3000 K. Since the aluminum splats act as binder entrapping the hard alumina particles, lack of aluminum likely causes poor cohesion of the coatings. In this study, 20 wt.% of alumina was proven to be the appropriate proportion for the cost-effective Al-based coatings with favorable anti-corrosion and wear properties. The novel coatings have great potential for protecting marine structures.

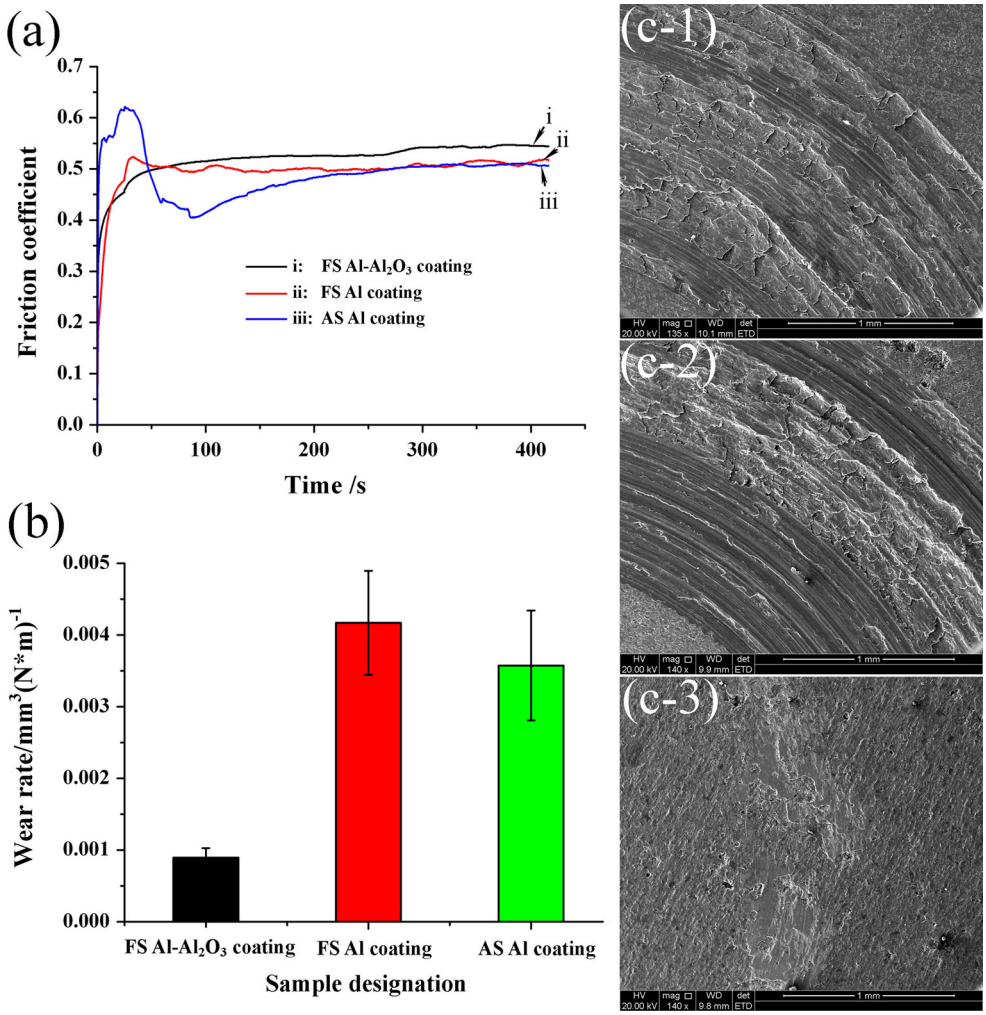

Fig. 6 Wear testing results for the coatings, (a) friction coefficient curves, (b) wear rate of the coatings, and (c) FESEM views of the worn surfaces of the coatings suggesting the different wear regimes (c-1: the AS Al coating, c-2: the FS Al coating, and c-3: the FS Al-Al_2O_3 coating)

4. Conclusions

Dense aluminum-alumina composite coatings have been successfully fabricated by flame spraying. The evenly distributed alumina splats in the coatings formed a hard skeleton structure. The novel structure brought about by the addition of alumina gave rise to significantly enhanced anti- wear and corrosion performances of the coatings. The cost-effective flame sprayed novel Al-Al_2O_3 composite coatings is promising for potential applications as the barrier and sacrificial protective layers in the marine environment.

Acknowledgements

This research was supported by the National Natural Science Foundation of China (Grant # 31271017) and 100 Talents Program of Chinese Academy of Sciences (both to H.L.).

References

1. R.E. Melchers, Long-Term Corrosion of Cast Irons and Steel in Marine and Atmospheric Environments, *Corros. Sci.*, 2013, **68**, p 186-194
2. W.M. Zhao, Y. Wang, C. Liu, L.X. Dong, H.H. Yu, and H. Ai, Erosion-Corrosion of Thermally Sprayed Coatings in Simulated Splash Zone, *Surf. Coat. Technol.*, 2010, **205**(7), p 2267-2272
3. B.R. Hou, *Ocean Environment Corrosion Theory and Its Application*, 1st ed., B. Peng, Ed., Science Press, 1999, p 199
4. Y. Bai, Q. Bai, *Subsea Pipelines and Risers*, 2nd ed., Elsevier Science Ltd., 2005, p 229
5. K.L. Money, Corrosion Testing in the Atmosphere, *Metals Handbook*, 9th ed., ASM International, Materials Park, 1987, p 49
6. D.P. Schmidt, B.A. Shaw, E. Sikora, W.W. Shaw, and L.H. Laliberte, Corrosion Protection Assessment of Sacrificial Coating Systems as a Function of Exposure Time in a Marine Environment, *Prog. Org. Coat.*, 2006, **57**(4), p 352-364
7. B.S. Phull and W.W. Kirk, Monitoring the Corrosivities of Atmospheric Exposure Sites, *J. Prot. Coat. Linings*, 1991, **8**(1), p 152-162
8. J.A. Ellor, W.T. Young, and J. Repp, *Thermally Sprayed Metal Coatings to Protect Steel Pilings: Final Report and Guide*, NCHRP Report, Washington DC, 2004, p 7

9. M. Matsumoto, N. Okada, K. Nishihara, K. Kimoto, T. Kudo, and S. Fujimoto, Corrosion Products near the Shear Cut Edge of Steel Sheets Coated with 55 wt.% Al-Zn Alloy in a Simulated Marine Atmospheric Environment, *Corros. Eng.*, 2010, **59**(12), p 382-396
10. R. Selvaraj, M. Selvaraj, and S.V.K. Yer, Studies on the Evaluation of the Performance of Organic Coatings Used for the Prevention of Corrosion of Steel Rebars in Concrete Structures, *Prog. Org. Coat.*, 2009, **64**(4), p 454-459
11. S. Kuroda, J. Kawakita, and M. Takemoto, An 18-year Exposure Test of Thermal-Sprayed Zn, Al, and Zn-Al Coatings in Marine Environment, *Corrosion*, 2006, **62**(7), p 635-647
12. J. Kawakita, S. Kuroda, T. Fukushima, and T. Kodama, Corrosion Resistance of HVOF Sprayed HastelloyC Nickel Base Alloy in Seawater, *Corros. Sci.*, 2003, **45**(12), p 2819-2835
13. K.S. Tan, J.A. Wharton, and R.J.K. Wood, Solid Particle Erosion-Corrosion Behaviour of a Novel HVOF Nickel Aluminium Bronze Coating for Marine Applications-Correlation Between Mass Loss and Electrochemical Measurements, *Wear*, 2005, **258**(11-12), p 629-640
14. S. Armada, B.G. Tilset, M. Pilz, R. Liltvedt, H. Bratland, and N. Espallargas, Sealing HVOF Thermally Sprayed WC-CoCr Coatings by Sol-Gel Methods, *J. Therm. Spray Technol.*, 2011, **20**(4), p 918-926
15. Y. Wang, Y.G. Zheng, W. Ke, W.H. Sun, W.L. Hou, X.C. Chang, and J.Q. Wang, Slurry Erosion-Corrosion Behaviour of High-Velocity Oxy-Fuel (HVOF) Sprayed Fe-Based Amorphous Metallic Coatings for Marine Pump in Sand-Containing NaCl Solutions, *Corros. Sci.*, 2011, **53**(10), p 3177-3185
16. D. Chaliampalias, G. Vourlias, E. Pavlidou, G. Stergioudis, S. Skolianos, and K. Chrissafis, High Temperature Oxidation and Corrosion in Marine Environments of Thermal Spray Deposited Coatings, *Appl. Surf. Sci.*, 2008, **255**(5), p 3104-3111
17. F.S. Rogers, Thermal Spray for Commercial Shipbuilding, *J. Therm. Spray Technol.*, 1997, **6**(3), p 291-293
18. A.J. Speyer, Wear-Corrosion Sensing in Flowing Seawater, Ph.D. Thesis, School of Engineering Sciences, University of Southampton, November 2002
19. S. Kuroda, J. Kawakita, and M. Takemoto, *Thermal Spray Committee, Marine Exposure Tests of Thermal Sprayed Coatings in Japan, Thermal Spray 2003: Advancing the Science and Applying the Technology*. C. Moreau, B. Marple, Eds., ASM International. Materials Park, OH, 2003
20. R.J.K. Wood, B.G. Mellor, and M.L. Binfield, Sand Erosion Performance of Denotation Gun Applied Tungsten Carbide/Cobalt-Chromium Coatings, *Wear*, 1997, **211**(1), p 70-83
21. B. Szczygieł and M. Kołodziej, Corrosion Resistance of Ni/Al_2O_3 Coatings in NaCl Solution, *Trans. Inst. Met. Finish.*, 2005, **83**(4), p 181-187
22. J.R. Scully, A. Lucente, Corrosion of Amorphous Metals. *ASM Handbook. Corrosion: Materials*, Vol. 13B, S.D. Cramer, B.S. Covino Jr., Eds., ASM International, Materials Park, OH, 2005, p 476-489
23. D. Lopez, J.P. Congote, J.R. Cano, A. Toro, and A.P. Tschiptschin, Effect of Particle Velocity and Impact Angle on the Corrosion-Erosion of AISI, 304 and AISI, 420 Stainless Steels, *Wear*, 2005, **259**(1-6), p 118-124
24. A.M. Fan, J.M. Long, and Z.Y. Tao, An Investigation of the Corrosive Wear of Stainless Steels in Aqueous Slurries, *Wear*, 1996, **193**(1), p 73-77
25. A. Neville, T. Hodgkiess, and J.T. Dallas, A Study of the Erosion-Corrosion Behavior of Engineering Steel for Marine Pumping Applications, *Wear*, 1995, **187-187**(Part 2), p 497-507
26. L. Esposito and A. Tucci, Microstructural Dependence of Friction and Wear Behaviours in Low Purity Alumina Ceramics, *Wear*, 1997, **205**(1-2), p 88-96
27. K. Poser, K.H.Z. Gahr, and J. Schneider, Development of $A1_2O_3$ Based Ceramics for Dry Friction Systems, *Wear*, 2005, **259**(1-6), p 529-538
28. ASTM B 117/90: Standard Test method of Sal Spray (FOG) Testing, 1990, p 19
29. Z.X. Tai, Y.F. Chen, Y.F. An, X.B. Yan, and Q.J. Xue, Tribological Behavior of UHMWPE Reinforced with Graphene Oxide Nanosheets, *Tribol. Lett.*, 2012, **46**(1), p 55-63
30. M.D. Wang and L.L. Shaw, Effects of the Powder Manufacturing Method on Microstructure and Wear Performance of Plasma Sprayed Alumina-Titania Coatings, *Surf. Coat. Technol.*, 2007, **202**(1), p 34-44
31. L.L. Shaw, D. Goberman, R.M. Ren, M. Gell, S. Jiang, Y. Wang, T.D. Xiao, and P.R. Strutt, The Dependency of Microstructure and Properties of Nanostructured Coatings on Plasma Spray Conditions, *Surf. Coat. Technol.*, 2000, **130**(1), p 1-8
32. R.M.H.P. Rodriguez, R.S.C. Paredes, S.H. Wido, and A. Calixto, Comparison of Aluminum Coatings Deposited by Flame Spray and by Electric Arc Spray, *Surf. Coat. Technol.*, 2007, **202**(1), p 172-179
33. R. Bhaskaran, N. Palaniswamy, N.S. Rengaswamy, and M. Jayachandran, Global Cast of Corrosion-A Historical Review, in *ASM Handbook*, Vol. 13B, Corrosion: Materials, ASM International, Materials Park, OH, 2005, p 621-628
34. I. Garcia, A. Conde, G. Langelaan, J. Fransaer, and J.P. Celis, Improved Corrosion Resistance Through Microstructural Modifications Induced by Codepositing SiC-Particles with Electrolytic Nickel, *Corros. Sci.*, 2000, **45**(6), p 1173-1189
35. S. Maitra and G.C. English, Mechanism of Localized Corrosion of 7075 Alloy Plate, *Metall. Mater. Trans. A*, 1981, **12**(3), p 535-541
36. M.R. Barbosa, J.A. Bastos, J.J. Garcia-Jareno, and F. Vicente, Chloride Role in the Surface of Nickel Electrode, *Electrochim. Acta*, 1998, **44**(6-7), p 957-965
37. M. Trueba and S.P. Trasatti, Study of Al Alloy Corrosion in Neutral NaCl by the Pitting Scan Technique, *Mater. Chem. Phys.*, 2010, **121**(3), p 523-533
38. Y.S. Zoo, J.W. An, D.P. Lim, and D.S. Lim, Effect of Carbon Nanotube Addition on Tribological Behavior of UHMWPE, *Tribol. Lett.*, 2004, **16**(4), p 305-309
39. R.G. Kelly, J.R. Scully, D.W. Shoesmith, and R.G. Buchheit, *Electrochemical Techniques in Corrosion Science and Engineering*, Chap. 8. Marcel-Dekker, New York, 2003, p 296-298
40. S.T. Aruna, V.E. Selvi, V.K.W. Grips, and K.S. Rajam, Corrosion- and Wear-Resistant Properties of Ni-Al_2O_3 Composite Coatings Containing Various Forms of Alumina, *J. Appl. Electrochem.*, 2011, **41**(4), p 461-468
41. A.R. Molla, B.V.M. Kumar, and B. Basu, Friction and Wear Mechanisms of K_2O-B_2O_3-Al_2O_3-SiO_2-MgO-F Glass-Ceramics, *J. Eur. Ceram. Soc.*, 2009, **29**(12), p 2481-2489
42. J. Park, S.H. You, D.W. Shin, and A. Ozturk, Tribological Behavior of Alumina-Added Apatite-Wollastonite Glass-Ceramics in Simulated Body Fluid, *Mater. Chem. Phys.*, 2010, **124**(1), p 113-119